

A non-destructive technique for chemical mapping of insect inclusions in amber

Anezka Popovski Kolaceke ^{Corresp., 1}, Ryan C McKellar ^{2,3}, Mauricio Barbi ¹

¹ Physics Department, University of Regina, Regina, Saskatchewan, Canada

² Palaeontology, Royal Saskatchewan Museum, Regina, Saskatchewan, Canada

³ Biology Department, University of Regina, Regina, Saskatchewan, Canada

Corresponding Author: Anezka Popovski Kolaceke

Email address: anezka@uregina.ca

Synchrotron-based techniques offer a wealth of elemental, molecular, and structural insights in biological samples, but the application of these techniques to fossils is a relatively new development. Here we examine how Synchrotron Radiation Micro X-Ray Fluorescence (SR μ XRF) provides insights into the chemical composition of insects trapped in amber, while leaving the inclusions unaltered. By analyzing a series of ants (Hymenoptera: Formicidae) that range from modern material, to Eocene Baltic amber, and Late Cretaceous North Carolina amber, we investigate how variable preservation influences the results obtained through SR μ XRF analyses, as well as the various merits and pitfalls associated with the application of this technique to amber inclusions. The initial results from this line of research are encouraging. They provide new avenues to study elements that are original to the specimens involved, as well as those generated through decay, or introduced during taphonomic processes. This new technique also suggests a range of complementary techniques that may allow future studies to pursue traces of original colour and cuticular reinforcement in amber inclusions. Ultimately, this work serves as an introduction to the underlying principles, strengths, and limitations associated with applying SR μ XRF in a palaeontological context.

1 **A non-destructive technique for chemical mapping of insect inclusions in**
2 **amber**

3

4 Anezka Popovski Kolaceke¹, Ryan C. McKellar^{2,3}, Mauricio Barbi¹

5

6 ¹ Physics Department, University of Regina, Regina, Saskatchewan, Canada

7 ² Palaeontology, Royal Saskatchewan Museum, Regina, Saskatchewan, Canada

8 ³ Biology Department, University of Regina, Regina, Saskatchewan, Canada

9

10 Corresponding Author:

11 Anezka Popovski Kolaceke¹

12

13

14 Email address: anezkakolaceke@gmail.com

15

16

17

18

19

20

21

22

23

24

25

26

27

28

29

30

31

32

33

34

35

36

37

38

39

40

41

42

43 Abstract:

44 Synchrotron-based techniques offer a wealth of elemental, molecular, and structural insights in
45 biological samples, but the application of these techniques to fossils is a relatively new
46 development. Here we examine how Synchrotron Radiation Micro X-Ray Fluorescence (SR
47 μ XRF) provides insights into the chemical composition of insects trapped in amber, while
48 leaving the inclusions unaltered. By analyzing a series of ants (Hymenoptera: Formicidae) that
49 range from modern material, to Eocene Baltic amber, and Late Cretaceous North Carolina amber,
50 we investigate how variable preservation influences the results obtained through SR μ XRF
51 analyses, as well as the various merits and pitfalls associated with the application of this
52 technique to amber inclusions. The initial results from this line of research are encouraging. They
53 provide new avenues to study elements that are original to the specimens involved, as well as
54 those generated through decay, or introduced during taphonomic processes. This new technique
55 also suggests a range of complementary techniques that may allow future studies to pursue traces
56 of original colour and cuticular reinforcement in amber inclusions. Ultimately, this work serves
57 as an introduction to the underlying principles, strengths, and limitations associated with
58 applying SR μ XRF in a palaeontological context.

59

60 Key words: synchrotron, x-ray fluorescence, fossil, preservation, Formicidae, amber, imaging,
61 palaeontology

62

63 1. Introduction:

64 Synchrotron radiation has been utilized in the study of fossil insects for over a decade (Tafforeau
65 et al., 2006). However, most of these analytical efforts have been focussed on morphology,
66 making use of techniques such as synchrotron radiation x-ray microtomography (SR x-ray μ CT).
67 This technique has shed new light on fossil insects trapped in nearly opaque amber (Lak et al.,
68 2008), and on structures within insects and arthropods that are highly informative in terms of
69 their evolutionary relationships, or palaeoecology (e.g., Kirejtshuk et al., 2009; Edgecombe et al.,
70 2012; Henderickx et al., 2013). A recent review of these efforts has been conducted by Soriano et
71 al. (2010).

72 To date, few studies have examined chemistry within fossil insects using synchrotron
73 radiation. Fossils of vertebrates, such as avian and non-avian theropods, and reptiles have
74 received most attention (e.g., Bergmann et al., 2010; Edwards et al., 2011; Wogelius et al., 2011).
75 Because of the size of the samples involved, Synchrotron Rapid Scanning X-ray Fluorescence
76 (SRS-XRF) has been the primary technique utilized to map elemental distributions. The state of
77 the art for scanning larger specimens was recently reviewed in the work of Bergmann et al.
78 (2012). Analyses of smaller fossils, such as insects, have been limited to work with Scanning
79 Electron Microscopy (SEM), employing an Energy Dispersive Spectrometer (EDS) to probe
80 exposed compression fossils. Examples of this style of research include studies that have
81 searched for traces of vertebrate blood within the body cavities of biting insects in the Eocene
82 Kishenehn Formation (Greenwalt et al., 2013), or examined mineral replacement within the
83 insects of the Cretaceous Crato Formation, Brazil (Barling et al., 2015).

84 The focus on larger fossils in chemical mapping efforts utilizing synchrotron radiation
85 has created a situation in which the samples approached with leading-edge techniques often lack
86 the quality of preservation seen within amber deposits, because they are mainly compression
87 fossils (carbon films) or partially replaced (e.g., permineralized or diagenetically altered skeletal
88 material). Amber offers an unmatched degree of preservation, with some deposits preserving
89 mummified or partially carbonized soft tissues that are tens of millions of years old (Henwood,
90 1992a, 1992b; Grimaldi et al., 1994). The best examples of this degree of preservation are the
91 uncommon findings of muscle, brain, and glandular tissue within Dominican amber insects
92 (Henwood, 1992b; Grimaldi et al., 1994), and rare occurrences of muscle tissue preserved within
93 Baltic amber insects (Van de Kamp et al., 2014). Previous works have examined tissues through
94 ‘crack-out’ studies, where the amber is split in order to sample the inner cavities of insect
95 inclusions. These destructive techniques have provided exceptional scanning electron
96 microscopy (SEM) images of various tissues, and have created the opportunity for Transmission
97 Electron Microscopy (TEM) or chemical observations of extracted tissues (Henwood, 1992b;
98 Grimaldi, 1994). However, these techniques rely on damaging specimens, and there are no
99 definitive external indicators for soft tissue preservation before a specimen is split. Utilizing
100 Synchrotron Radiation Micro X-Ray Fluorescence (SR μ XRF) permits the exploration of fossils
101 as small as insect inclusions. The technique also holds much promise for investigating other
102 fossils with exceptional preservation at a micrometre scale (e.g., McNamara et al., 2010).

103 To date, the closest approach to a non-destructive technique for examining the makeup of
104 amber inclusions has been the use of Confocal Laser Scanning Microscopy (CLSM). This
105 technique has been used to study fossil fungi and plant trichomes with great success (e.g.,
106 Speranza et al., 2010, Clark and Daly, 2010). However, CLSM relies heavily on autofluorescence
107 of biological samples in amber. The range of energies utilized (and therefore molecules
108 examined) is restricted by the wavelengths of laser light employed, and in many deposits the
109 amber itself autofluoresces, producing a masking effect. SR μ XRF does not suffer from these
110 particular drawbacks, but the technique has its own limitations, which we describe below.

111 The samples used in this study are comprised of ants (Hymenoptera: Formicidae) ranging
112 from recent exemplars to those found in Eocene Baltic amber (~50 Ma: Weitschat and Wichard,
113 2010), and Cretaceous North Carolina amber (~83.6 to 72.1 Ma: Krynicky, 2013). This series of
114 samples was chosen to examine the fidelity with which amber preserves the original chemistry of
115 tissues and decay products. Modern analogues are compared to some of the oldest examples of
116 soft tissue preservation available within amber (Baltic amber), and to insects that belong to the
117 same family, but have progressed beyond the limits of soft tissue preservation (North Carolina
118 amber). This is an effort to lay the groundwork for analyses of additional elements across a wider
119 range of amber deposits and fossil taxa. It is also an attempt to introduce the palaeontological
120 community to the underlying principles, strengths, and caveats associated with using this form of
121 chemical analysis in fossil samples.

122

123 2. Materials & Methods:

124

125 2.1. Samples and Preparation

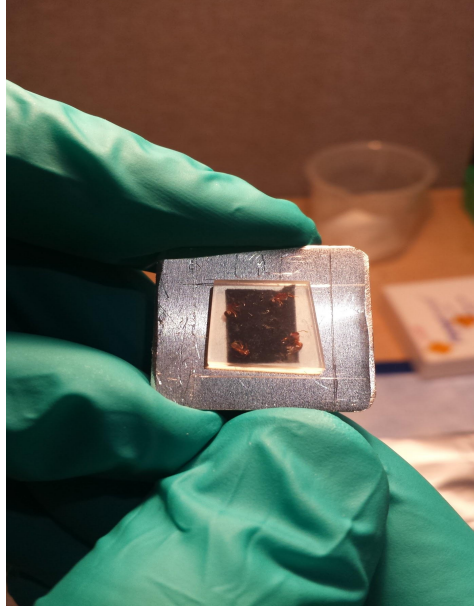
126 Each amber sample was embedded in mineralogical grade epoxy and cut with a water-cooled
127 lapidary saw, so that the amber layer between the surface and the insect was between one and
128 two millimetres thick. Subsequently, each specimen was polished with a series of lapidary
129 wheels and wet sanding baths, until the amber layer was as thin as possible without creating any
130 risk of causing damage to the insect (total specimen thickness was approximately two
131 millimetres in most cases). The overlying amber layer varied in thickness from sample to sample,
132 due to specimen and limb orientations, but this layer was typically in the range of tens to
133 hundreds of micrometres in thickness. In cases where the insect's appendages were directed
134 toward a polished surface in the preparation, a thicker layer of overlying amber was left in place
135 in an attempt to prevent infiltrations and damage to the samples. Once the amber pieces reached
136 the target size and before the data acquisition, they were cleaned using isopropanol: otherwise,
137 there was no other chemical pre-treatment. SR μ XRF measurements were taken from the epoxy
138 surrounding the samples, in order to ensure that no trace metals were present within the
139 mountant, and that the polishing and handling process had not introduced contaminants that may
140 influence sample observations.

141 Comparative ant samples were prepared by inserting modern ants into the same epoxy
142 resin that was used for amber embedding (Epo-Tek 301). Two treatments were attempted (live
143 and dead embedding), to observe any differences in interaction with resin. This was meant to
144 simulate different scenarios in which ants could end up trapped in resin, and to investigate any
145 differences in tissue impregnation as a result of these interactions. Once the resin solidified, the
146 samples were prepared with the same steps as the amber specimens. Museum specimens
147 included in this study came from the Royal Saskatchewan Museum Palaeontology Collections,
148 Regina, SK, Canada (RSM, P specimen prefixes); and the Division of Entomology, University of
149 Kansas Natural History Museum, Lawrence, Kansas (SEMC, NC 272-276).

150

151 2.2. Data Acquisition

152 The specimens were mounted using carbon tape, upon an aluminum sample holder at the Soft X-
153 ray Micro-characterization Beamline (SXRMB), at the Canadian Light Source (CLS) (Fig. 1).
154 Because the use of lower energy x-rays on this beamline requires experiments conducted in
155 vacuum (due to their low penetration in air), more than one specimen was often mounted at a
156 time, in order to save time at the beamline.



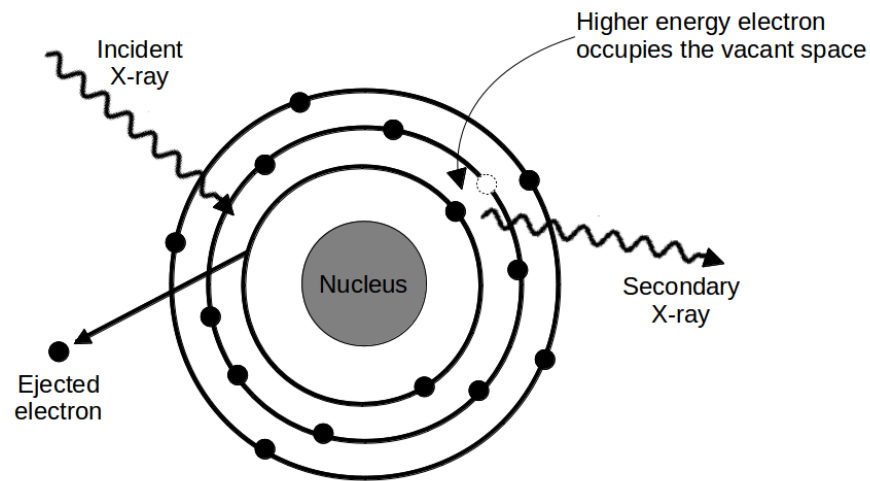
157

158 Fig. 1 - Modern ant samples mounted in an epoxy block, on aluminum sample holder (each ant is
159 near a corner of the carbon tape).

160

161

162 The analytical technique chosen was SR μ XRF, a form of x-ray fluorescence
163 spectroscopy where a sample is irradiated with x-rays, which interact with electrons, giving them
164 energy enough so they can move from lower to higher energy levels of atoms, or even be
165 completely removed from the atom (ionization process). When this happens, an electron
166 occupying a higher energy level will migrate to the vacant lower energy state, emitting a photon
167 with energy equivalent to the difference between the two energy states involved in the process
168 (Fig. 2). Given that the each atom has a well defined and unique set of energy levels, the emitted
169 photon will then act as a fingerprint of the atom in question. In a polyatomic sample, the
170 resulting data is an energy spectrum with a series of peaks. Each of these peaks corresponds to a
171 characteristic energy carried by photons emitted from a given atom, so that different elements
172 can be identified in the sample. In addition, the intensity of each peak is proportional to the
concentration of the corresponding element in the sample.



173

174 Fig. 2 - The X-Ray Fluorescence (XRF) process. An x-ray photon excites an electron in the atom
175 (left). Another electron, from a more energetic layer, occupies the empty space, releasing a
176 characteristic photon.

177

178

179

180

181

182

183

184

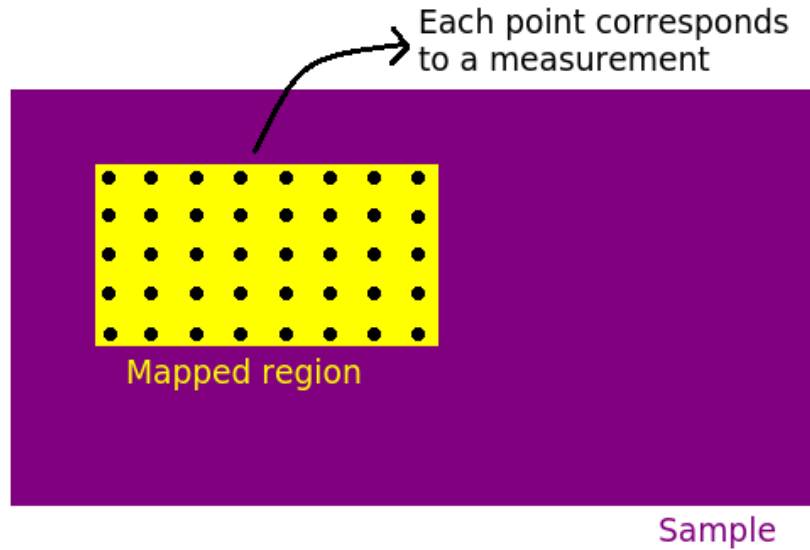
185

186

187

188

Using the default SXRMB beamline software, the scanning area in each sample was selected to cover the whole insect embedded in it; therefore the map size depended on the size of each ant (in some cases, when the area to be covered was deemed to be too large, the measurements were split between two maps of the specimen). In order to collect the data necessary to build an elemental map, each sample was moved in such a way that the x-ray beam probed “points” in the selected area in a series of well defined steps ($\sim 10 \mu\text{m}$) (Fig. 3), with each “point” being typically $\sim 10 \mu\text{m}$ in diameter. The fluorescence spectrum of each of these points was collected and used to produce the maps, as described in section 2.3. Table 1 shows the measurement parameters for each sample measured.



189

190

191

192

193 Table 1 - Data acquisition parameters for all samples analyzed.

Fig. 3 - Mapping with the SXRMB beamline software.

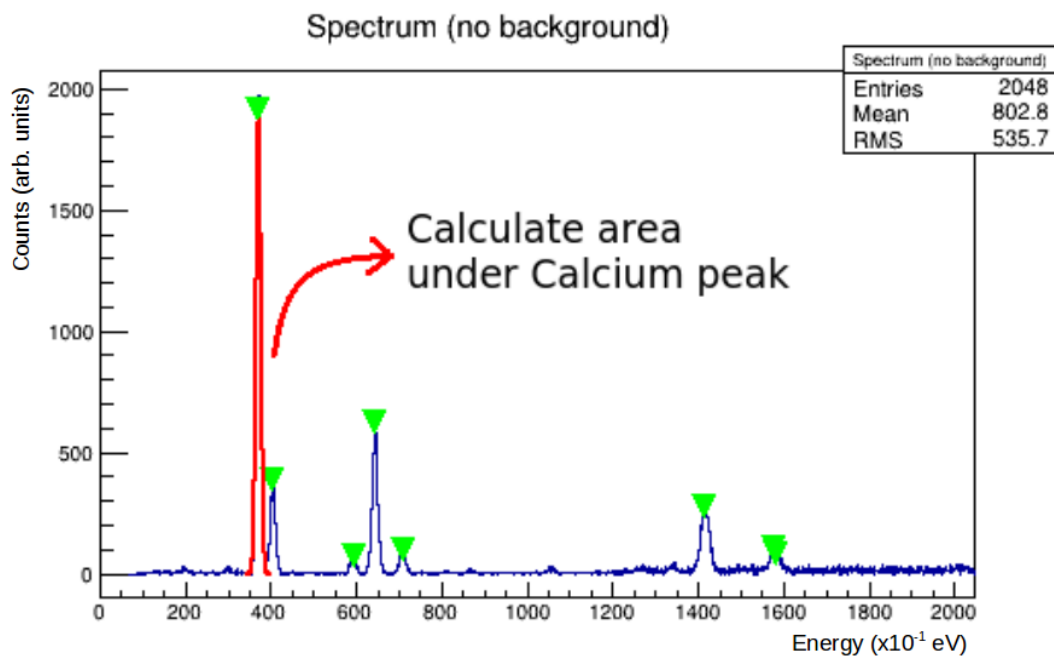
<i>Sample</i>	<i>Step size (μm)</i>	<i>Map size (mm)</i>	<i>Acquisition time (s)</i>	<i>Beam energy (eV)</i>
Modern ant	50.0 x 50.0	2.50 x 3.50	3.0	7200
Modern ant (dead)	60.0 x 60.0	2.60 x 1.90	2.0	7200
Baltic amber 6	40 x 40	4.00 x 2.90	4.0	7200
Baltic amber 13	45.0 x 45.0	2.40 x 3.20	3.0	7200
Baltic amber 8	40.0 x 40.0	2.40 x 2.10	3.0	7200
North Carolina amber	40.0 x 40.0	3.40 x 1.40 3.85 x 1.80	3.0	7200

194 2.3. Data Analysis Methodology

195 The methodology used to produce each map is discussed in this section.

196 A spectrum from a point in a given elemental map is shown in Fig. 4. As previously
197 discussed, different peaks refer to different elements. In order to generate the maps, an algorithm
198 was written using the CERN Root Data Analysis framework (Brun and Rademakers, 1996). This
199 software plots each spectrum and fits each peak using a Gaussian curve, as depicted in the Fig. 4
200 for calcium. Similar results can be obtained using the freely available software package PyMCA
201 (Solé et al., 2007).

202

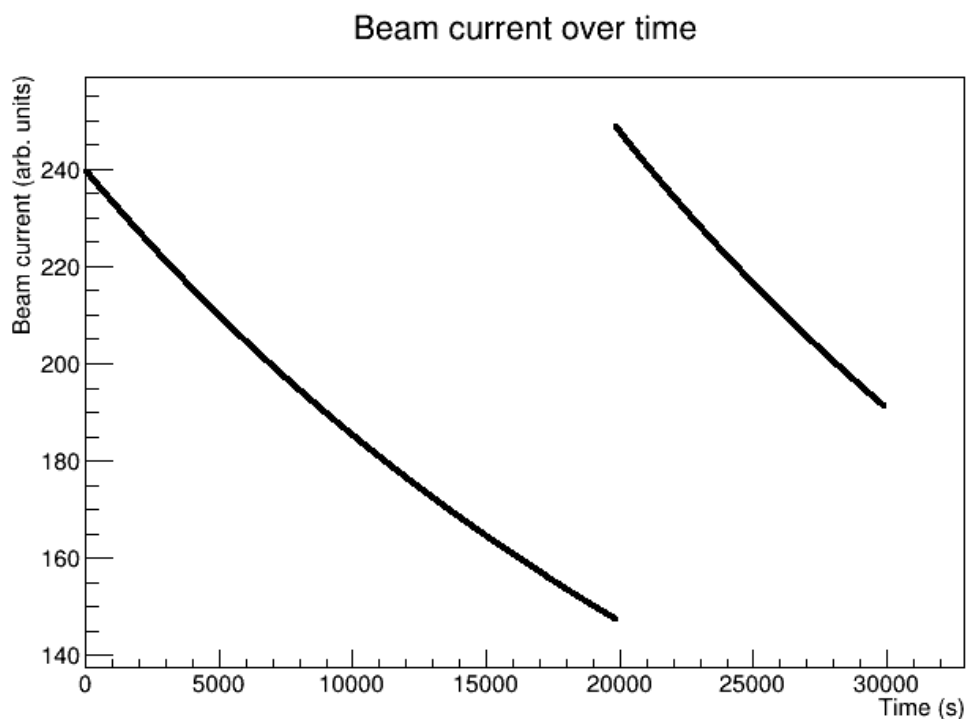


203

204 Fig. 4 - Spectrum from a single point in the map. The calcium peak is fitted with a Gaussian
205 curve. The area under this fitted peak is used to generate a point for the map of the element
206 (calcium in this figure). The green arrows show the different peaks identified with an automated
207 peak-finder algorithm.

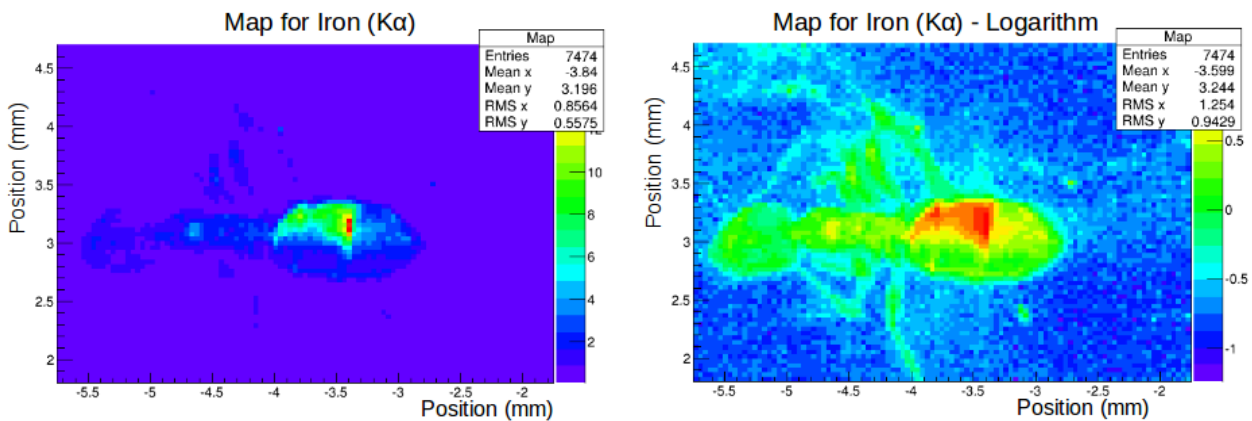
208

209 In order to translate the spectral data into a map that highlights chemical distributions, the
210 area under the peak corresponding to an element of interest is calculated using fitting parameters
211 for each spectrum (point) measured in the scanning procedure, resulting in a set of areas.
212 Corrections to the value of these areas are made to account for the variations in the intensity of
213 the synchrotron radiation beam during data collection (since the usual data acquisition takes
214 between 6 and 8 hours, the beam intensity can change significantly between the first and last
215 collected spectra, as can be observed in Fig. 5). The corrections are introduced by dividing the
216 values of each computed area by the beam current at the time when each corresponding spectrum
217 was collected. Each resulted area is then used as a representative of the concentration at each
218 point in the distribution map of that element in the sample.
219



220
221 Fig. 5 - Change in the beam current over the time elapsed to produce one chemical map. The
222 sudden rise in intensity at about 20000 seconds is due to a beam injection procedure performed
223 by the CLS accelerator group. Only the data acquisition time is considered in the figure. The
224 time intervals elapsed while moving the sample stage between two different points in the map are
225 not taken into account (no data acquisition occur during these intervals).

226 The elemental maps are bi-dimensional histograms where each point (similar to a pixel)
227 corresponds to a position on the irradiated side of the sample. The relative concentrations of each
228 element are represented using a colour scheme ranging from cold (towards blue) to warm
229 (towards red) indicating low to high values, respectively. In some cases, a few points have
230 concentrations much above the others, making it difficult to visualize the general elemental
231 distribution in the sample. To solve this problem, one can plot the logarithm of the normalized
232 areas instead of their original values. The difference between these two approaches can be noted
233 in Fig. 6.
234



235
236 Fig. 6 – Maps of an ant (specimen Ba 6, P3000.015) with a “hot spot” (area coloured in red) at
237 about (-2.5, 3.1) mm as shown using the absolute values of the normalized areas (left), and using
238 the logarithm of the normalized areas (right). The logarithm makes the small variations in
239 concentrations more visible, thus providing more details relative to the distribution of an element
240 (iron in this case) in the sample.
241

242 3. Results/Discussions:

243 3.1. Modern Ant

246 Elemental maps were plotted for the two specimens of modern ants as described in 2.1. The
247 maps, using logarithmic values for the normalized areas when necessary, are shown in Figures 7
248 and 8. Figure 7 depicts the ant that was introduced to resin while still alive, while figure 8 shows
249 the results for the ant that was encapsulated after death but prior to significant drying.

250

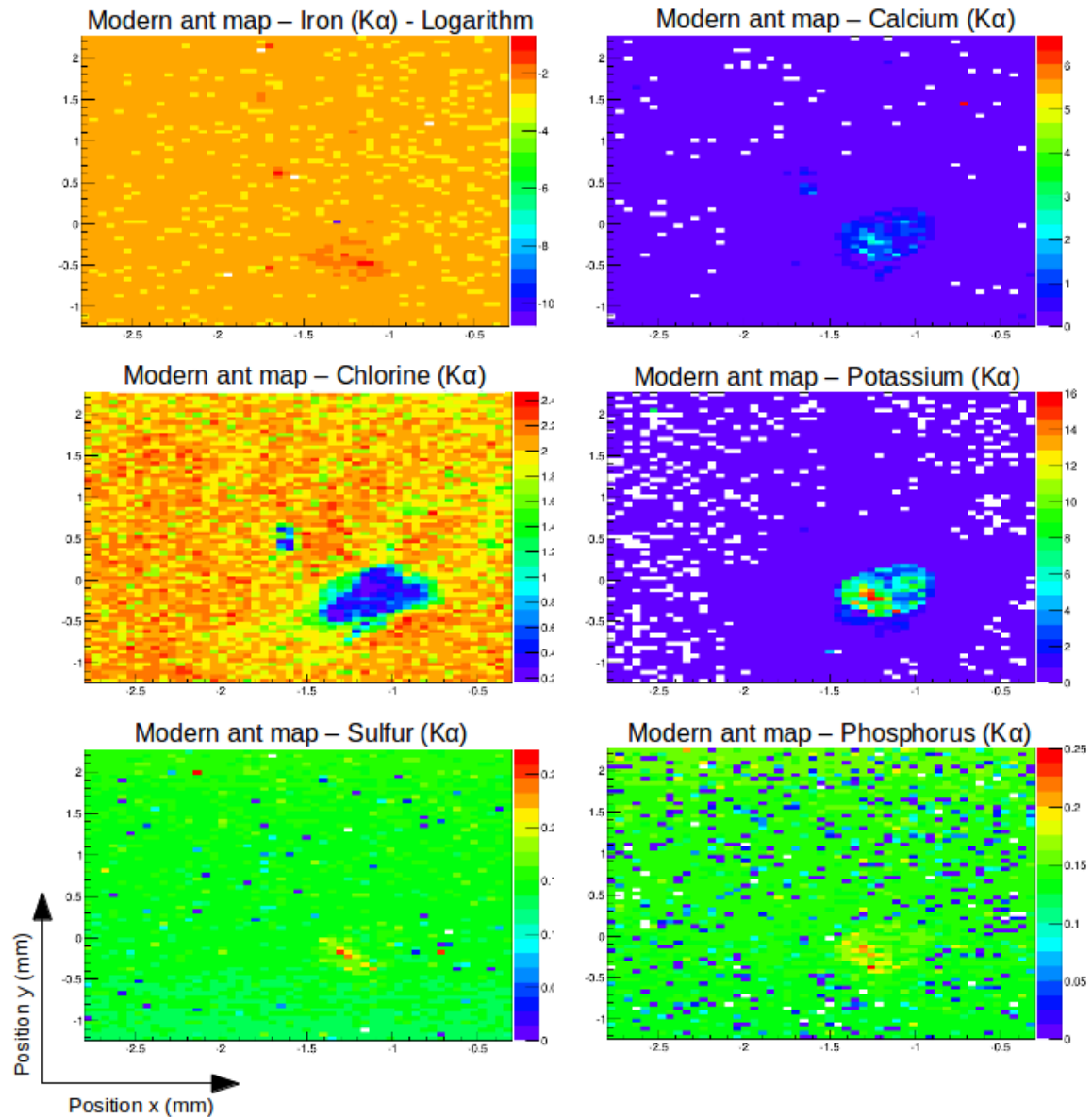
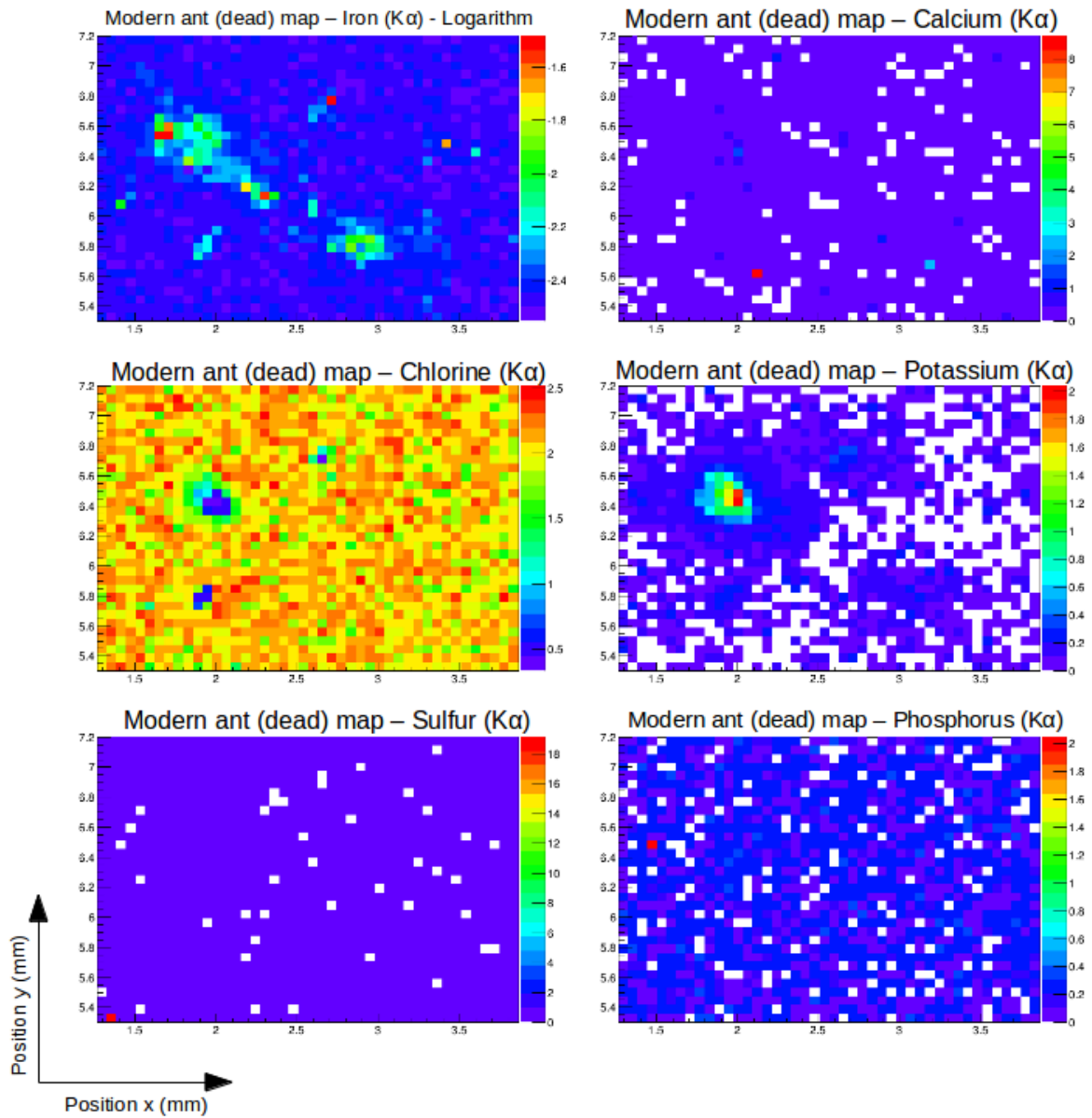
251
252
253
254

Fig. 7 - Maps for the live modern ant compared to its optical microscope image.

255



256

257

258

Fig. 8 - Maps for the dead modern ant compared to its optical microscope image.

259 The epoxy material used does not change the measured chemical composition of the ant
260 since the elements in its composition cannot be detected within the energy range used in the
261 measurements with SR μ XRF in the SXRMB beamline. The one exception is chlorine, which is
262 an impurity in the resin, but also it is not an element of interest within the insects. These
263 properties were verified by the measurement of a single point spectrum targeting the resin, which
264 provided no signal that could change the results presented herein. The presence of chlorine
265 almost exclusively in the resin can be seen on the maps, where it shows high concentrations
266 everywhere except in positions where the epoxy layer is very thin, (i.e., directly above the insect
267 inclusion). However, the *thickness* of the layer of epoxy (or amber) does play a role on the
268 resulting maps. As exemplified in Fig. 7, the fact that the ant is not positioned parallel with the
269 surface of the epoxy block, and perpendicular in relation to the beam, affects the results. In these
270 chemical maps, only the head of the ant is visible, because this is the part of the body with the
271 thinnest layer of epoxy overlying it. This particular analytical artefact is due to two penetration
272 effects: 1) the thicker the epoxy layer, the less x-rays will reach the ant in the first place; and, 2)
273 once the x-rays reach the ant, the fluorescence photons still have to travel through the epoxy in
274 order to reach the detector, so a thicker layer will attenuate this signal as well. These two effects
275 together may reduce the number of photons detected to the point where they are overwhelmed by
276 background and noise counts, and a measurement cannot be made. Since the thickness effect is
277 also present in amber samples, every effort should be made to orient insect inclusions parallel to
278 the upper sampling surface, and to achieve an overlying layer that is as thin as possible without
279 damaging the specimens in order to obtain the clearest mapping results possible.

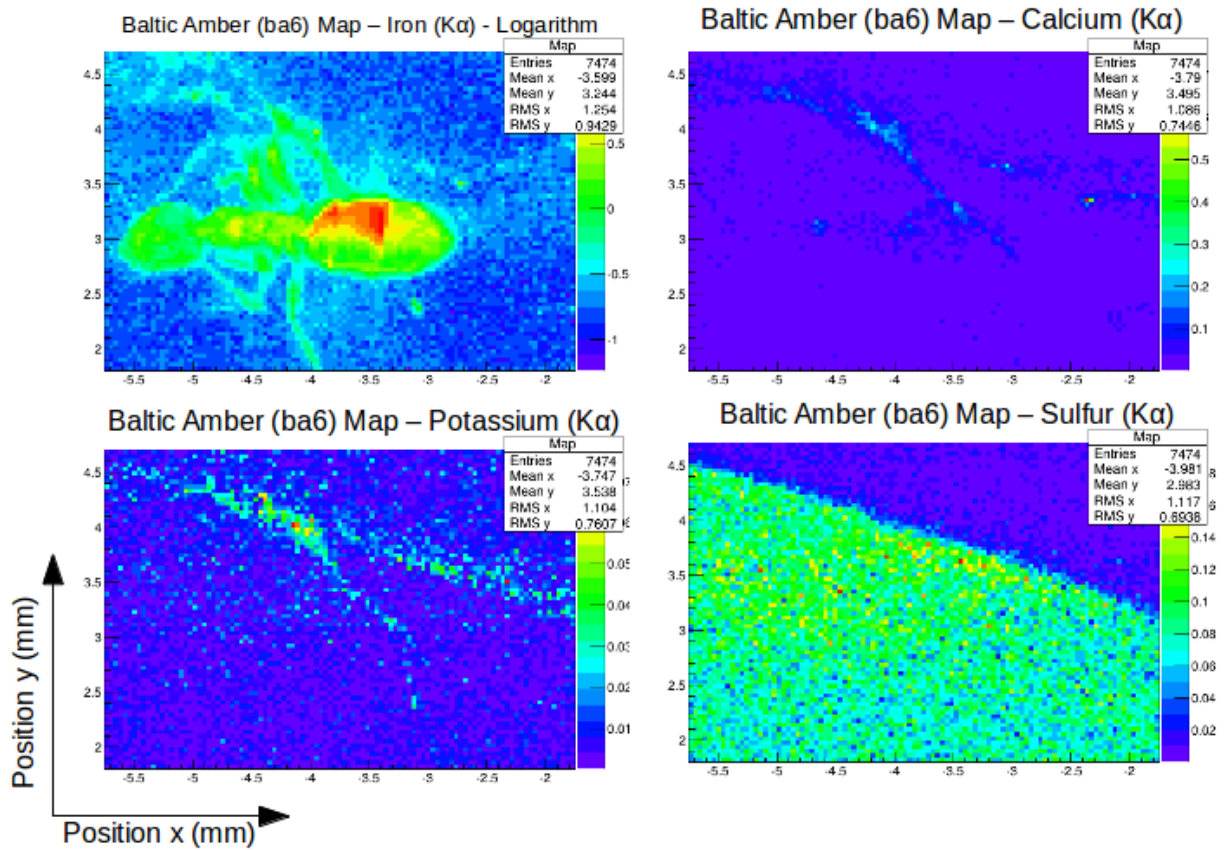
280 Although the effects of the thickness of the epoxy and amber layers on the quality of the
281 data are similar, the compositions of the two materials are different, with the epoxy containing a
282 larger amount of chlorine than the amber, as can be noted by comparing the results presented in
283 Fig. 7 and 8 with the results discussed in section 3.2. This difference should not heavily influence
284 analytical results in palaeontological studies because, as mentioned before, the distribution of
285 chlorine is not of particular interest within the insect inclusions, but it can be used to determine
286 physical properties of the amber itself. For example, the distribution of chlorine can be
287 informative in amber samples that have been embedded in epoxy for stabilization. In this case,
288 cracks that have been infilled by epoxy would show a much higher concentration of chlorine
289 than the adjacent areas.

290

291 3.2. Baltic Amber

292 Three specimens of ants in Baltic amber (P3000.015, P3000.016 and P3000.017) were mapped
293 and the plots are shown in Figs. 9, 10 and 11 (in logarithm scale). The maps in Fig. 9 were
294 generated using the data collected with an older version of the SXRMB beamline data
295 acquisition software. This older version did not provide the user with the data to plot each
296 spectrum, but only the area under the peaks corresponding to each selected element for each
297 point in the map. The consequence of this procedure was that only the maps for the elements
298 chosen at the data acquisition time were reconstructed, and that there was no control over the
299 algorithm used to produce the maps.

300



301

302

303

Fig. 9 - Maps for P3000.015 (specimen Ba 6) compared to its optical microscope image.

304

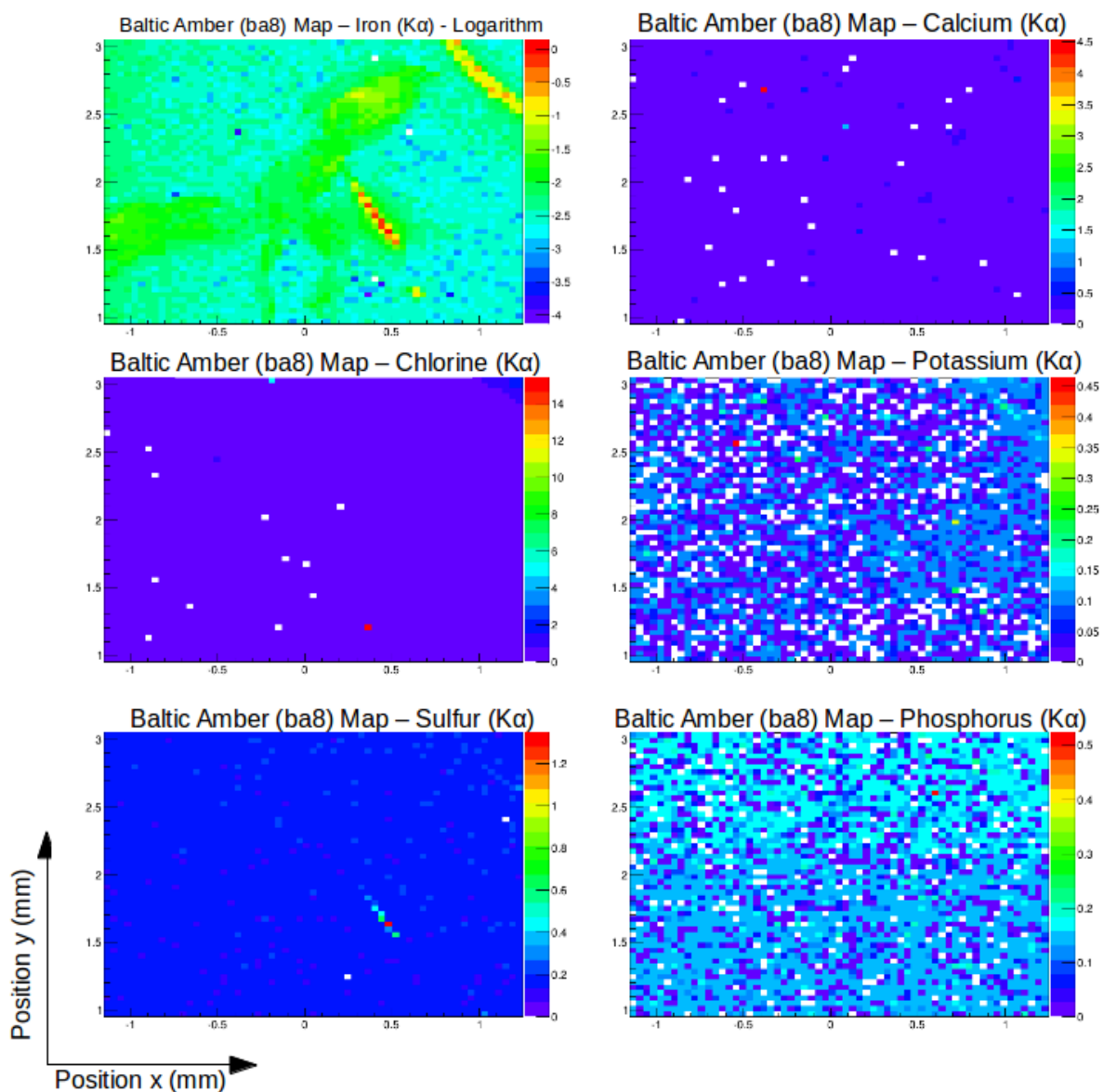
305
306
307

Fig. 10 - Maps for P3000.016 (specimen Ba 8) compared to its optical microscope image.

308

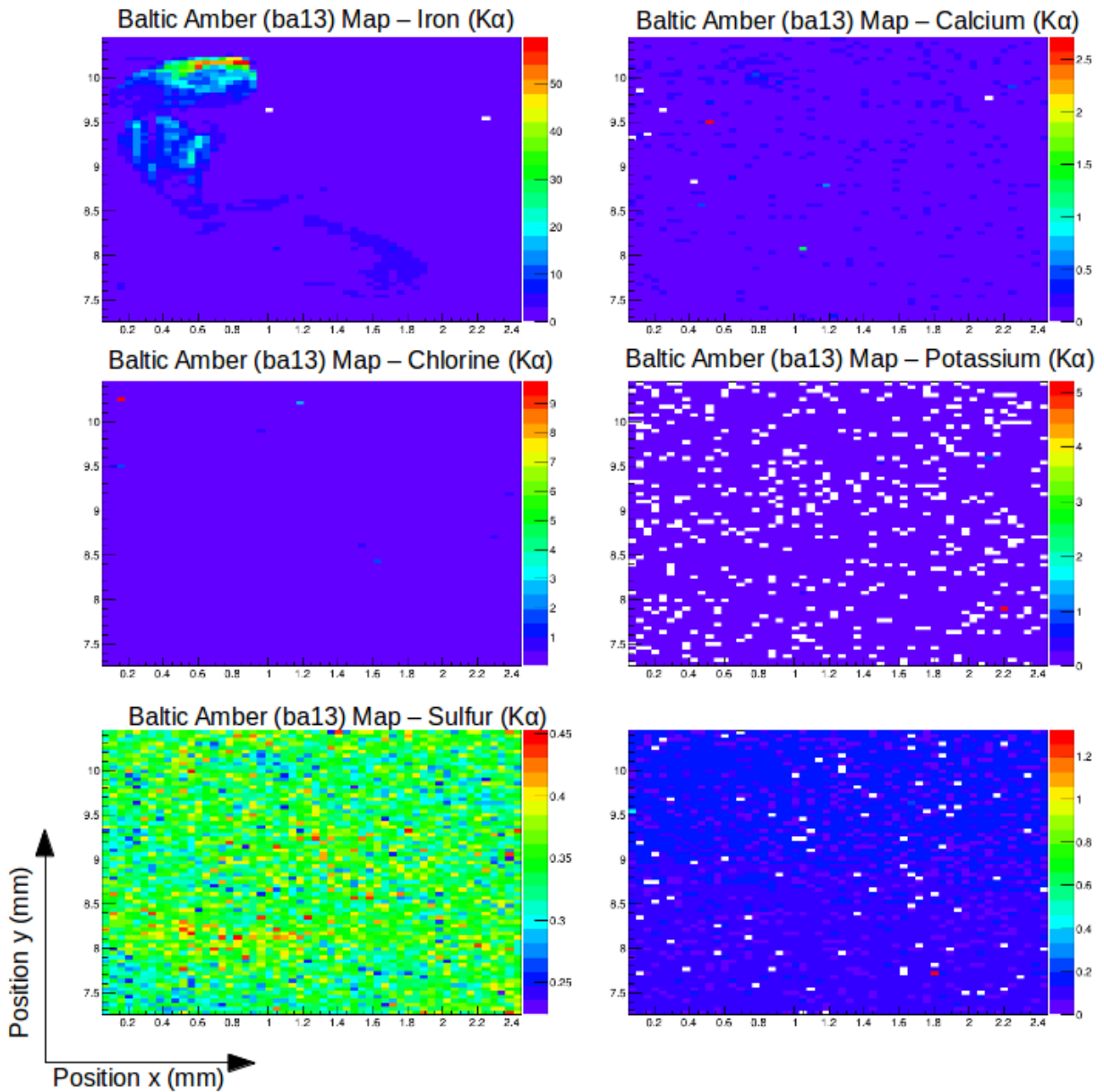
309
310

Fig. 11 - Maps for P3000.017 (specimen Ba 13) compared to its optical microscope image.

311 All the specimens show a clear distribution of iron, which seems to be the best preserved
312 element. Differences in concentrations, however, can be due to several factors such as: relative
313 position of the insect relative to the x-ray beam direction; different levels of preservation within
314 different parts of the insect; presence of different tissues and/or organs or decay products. It is,
315 thus, useful to incorporate at least one additional imaging technique that can add detailed
316 structural and positional information regarding the insect. For this purpose and as an extension of
317 the current study, we are currently collecting and analysing data using Synchrotron Radiation X-
318 ray micro-CT to assess the preservation of different tissues in some of the ant specimens
319 examined herein. This will allow us to overlay chemical and structural data to further the studies
320 presented in this work.

321 Iron is a material with biological relevance for insects. It is present in large quantities
322 while insects are alive, and it is also retained as a product of their soft tissue decay after death.
323 The main difference between biologically sourced iron and that introduced during diagenesis is
324 its oxidation state. Although this is a possibility that has yet to be explored, it seems probable
325 that synchrotron radiation could also be used to infer the source of elements within fossils by
326 means of using X-ray Absorption Near Edge Structure (XANES), which provides information
327 about the chemical state of the elements. This analysis can usually be made at the same
328 beamlines where SR μ XRF is performed. A major caveat for the use of XANES to infer the
329 presence of original iron is that some minerals, such as pyrite, also contain ferrous iron.

330 Although XRF mapping is not usually a quantitative method, it provides valuable
331 distribution information that in general can outclass others provided by more conventional
332 methods for insect inclusions. It is also mostly non-destructive (it requires the amber to be
333 modified, but not the insect), and non-invasive. Minimal sample preparation is required, with the
334 main concern related to the thickness of the amber layer between the insect and the x-ray beam.
335 Potential exists to use this technique in a semi-quantitative fashion, but this would require
336 comparisons between the samples being analyzed and standards (an example of such an attempt
337 can be seen on Tolhurst et al., 2015). However, it is difficult to envision this approach in the
338 context of non-destructive amber research, because of the range of sample thicknesses,
339 orientations, and chemical heterogeneity that are present within this setting.

340

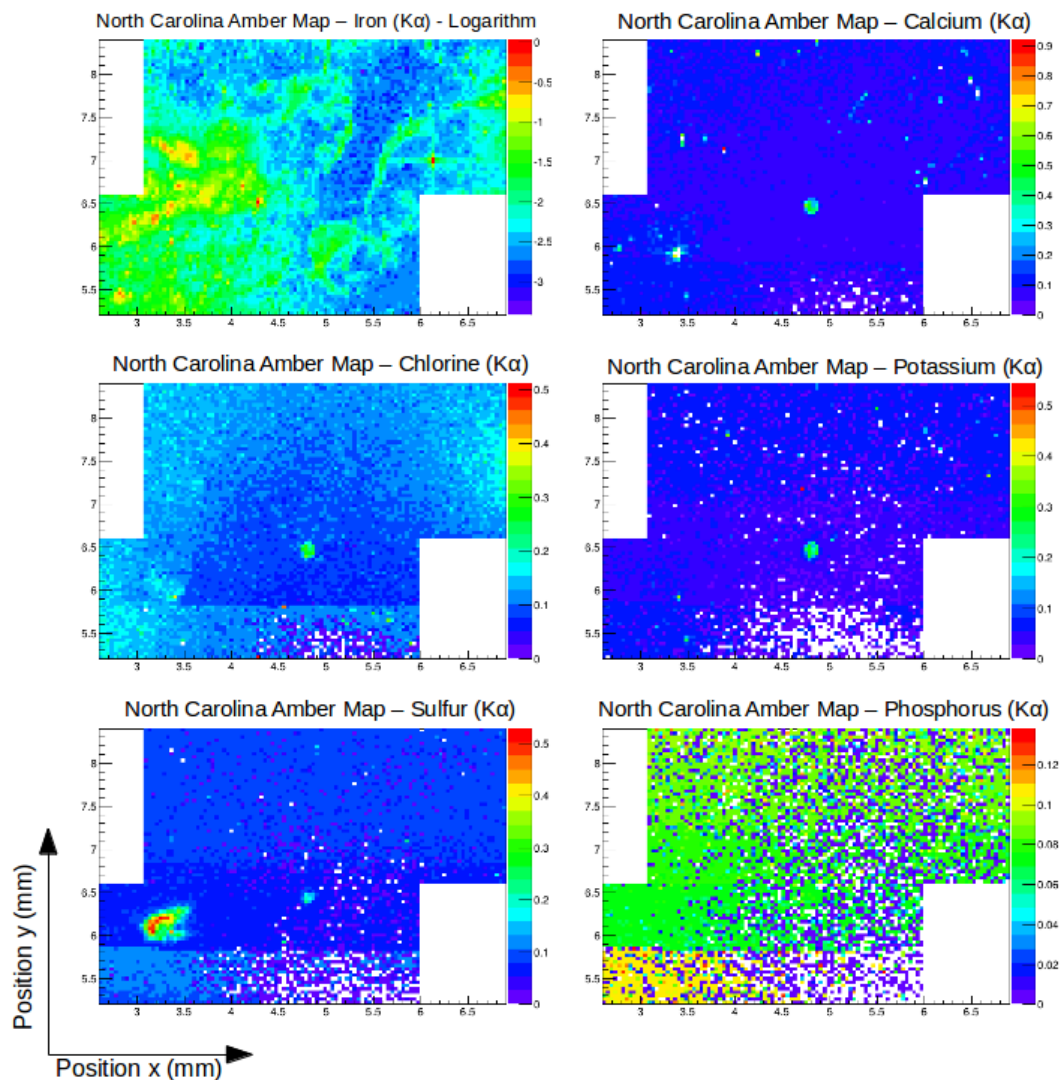
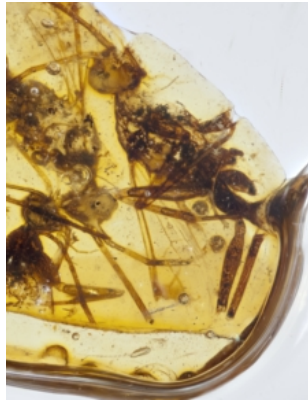
341

342 3.3. North Carolina Amber

343 The North Carolina amber specimen (NC 272-276) contains five partial ant inclusions, one of
344 which was mapped (Fig. 12). The choice of the inclusion to be mapped was made based on
345 preliminary x-ray images provided by a benchtop μ CT (Cooper Lab, University of
346 Saskatchewan). The ant selected was the specimen that showed the greatest contrast in the
347 benchtop analyses.

348

349



350
351
352
353
354

Fig. 12 - Maps for NC 272-276 compared to its optical microscope image. These maps are collages of the results of two scans, in different areas of the insect. The white rectangles represent the non-mapped areas. This method reduces the time it takes to measure the whole insect.

355 Although it is possible to see somewhat of an iron distribution, the insect is not as clearly
356 outlined as those seen in the elemental maps for the Baltic amber specimens, making the
357 interpretation of the results more difficult. This difference can be explained by the state of
358 preservation of the insect. Compared to the Baltic amber specimens, the specimens found in
359 North Carolina amber are much older, and the exoskeletons are not so well preserved. In the
360 Cretaceous material, each exoskeleton has become carbonized, and broken up into sheets of
361 cuticle that have a much lower concentration of iron. Even without chemical data, it is possible
362 to see that the insects have been heavily altered when compared to the specimens measured in
363 3.2. However, it appears as though some traces of the iron content within their original cuticle
364 stayed trapped within their carbonized remains.

365 Another obstacle encountered in the SR μ XRF analysis of the North Carolina amber
366 sample (which decreases the quality of the collected data), is the fact that the amber piece has a
367 curved outer surface. In this case, there was no way in which the amber piece could be polished
368 flat without damaging the insect inclusions. The problem with round samples is that not only is
369 the amber layer on top of the insect variable in thickness due to sample curvature, but the beam
370 can only be focused at one distance when the data for the map are being collected. A rounded
371 outer surface means that the beam focal distance should change in order to maintain focus on the
372 exoskeleton. Since the focal distance did not change during the course of our scans, there may be
373 additional uncertainties to the results of the scan. In particular, variable thickness and focal
374 distances may lower the quality of the measurements, or even add structures that do not reflect
375 real differences in the distribution of the elements, but rather geometric effects.

376
377

378 **4. Conclusions:**

379 Measuring chemical properties of amber inclusions in a non-destructive and non-invasive way is
380 possible using synchrotron radiation, as long as the insect is well preserved, and can be prepared
381 in an appropriate manner. In all of the well-preserved insects that we have examined to date, a
382 good iron distribution can be observed, and this distribution appears to be directly related to the
383 original cuticle, tissue, or decay products of the insect.

384 Moving forward, the best measurements will be the result of making sure the insect is as
385 flat as possible in relation to the x-ray beam and that the sample is polished parallel to the insect.
386 Curvatures or angles can interfere with beam focusing and beam penetration, and thus generate
387 uncertainties and distribution patterns that are not reflective of the insect itself. When
388 considering which samples to analyze through SR μ XRF, factors such as age, diagenetic history,
389 deposit type, and inclusion type, among others should be taken into account. These factors can
390 affect the preservation state of the insect, and they can dramatically alter the possibility of
391 obtaining good measurements from fossil specimens.

392 Future work will include chemical state analyses, using synchrotron techniques such as
393 XANES, so it will be possible to determine if the iron being measured is introduced, a product of
394 decay, or if it is original to the insect. Also, a different beamline, which can reach higher levels of
395 energy, could provide insights into the distribution of copper and zinc, which could give
396 information about the insect with respect to its cuticular reinforcement or colour, for example.

397

398 **Acknowledgements**

399

400 The authors thank David Cooper, Isaac Pratt, and Kim Harrison (University of Saskatchewan)
401 for assistance in benchtop x-ray μ CT scanning of amber inclusions in preparation for this project;
402 thanks are also given to Michael Engel (University of Kansas) and Victor Krynicki, for access to
403 the North Carolina ant specimens. The research described in this paper was performed at the
404 Canadian Light Source. Anezka P. Kolaceke acknowledges the receipt of support from the
405 Canadian Light Source Graduate Student Travel Support Program and from the Faculty of
406 Graduate Studies and Research at the University of Regina.

407

408 **References**

- 409 Barling N, Martill DM, Heads SW, Gallien S. 2014. High fidelity preservation of fossil insects
410 from the Crato Formation (Lower Cretaceous) of Brazil. *Cretaceous Research* 52:605-
411 622.
- 412 Bergmann U, Morton RW, Manning PL, Sellers WI, Farrar S, Huntley KG, Wogelius RA, Larson
413 P. 2010. *Archaeopteryx* feathers and bone chemistry fully revealed via synchrotron
414 imaging. *Proceedings of the National Academy of Sciences* 107(20):9060-9065.
- 415 Bergmann U, Manning PL, Wogelius RA. 2012. Chemical mapping of paleontological and
416 archeological artifacts with synchrotron X-rays. *Annual Review of Analytical Chemistry*
417 5:361-389.
- 418 Brun R, Rademakers, F. 1997. ROOT - An Object Oriented Data Analysis Framework.
419 *Proceedings AIHENP'96 Workshop, Lausanne, Sep. 1996, Nucl. Inst. & Meth. in Phys.*
420 *Res. A* 389: 81-86. See also <http://root.cern.ch/>.
- 421 Clark ND, Daly C. 2010. Using confocal laser scanning microscopy to image trichome
422 inclusions in amber. *Journal of Paleontological Techniques* 8:1-7.
- 423 Dietz W, Richter W, Schäfer U, Schmidt A. 2003. Investigation of microfossils in 100 million-
424 year-old amber. *Microscopy and Microanalysis* 9(S03):472-473.
- 425 Edgecombe GD, Vahtera V, Stock SR, Kallonen A, Xiao X, Rack A, Giribet G. 2012. A
426 scolopocryptopid centipede (Chilopoda: Scolopendromorpha) from Mexican amber:
427 synchrotron microtomography and phylogenetic placement using a combined
428 morphological and molecular data set. *Zoological Journal of the Linnean Society*
429 166(4):768-786.

- 430 Edwards NP, Barden HE, Van Dongen BE, Manning PL, Larson PL, Bergmann U, Sellers WI,
431 Wogelius RA. 2011. Infrared mapping resolves soft tissue preservation in 50 million
432 year-old reptile skin. *Proceedings of the Royal Society of London B: Biological Sciences*
433 278(1722):3209-18.
- 434 Greenwalt DE, Goreva YS, Siljeström, SM, Rose T, Harbach RE. 2013. Hemoglobin-derived
435 porphyrins preserved in a Middle Eocene blood-engorged mosquito. *Proceedings of the*
436 *National Academy of Sciences USA* 110(1849):18496-18500.
- 437 Grimaldi D, Bonwich E, Delannoy M, Doberstein S. 1994. Electron microscopic studies of
438 mummified tissues in amber fossils. *American Museum Novitates* 3097:1-31.
- 439 Henderickx H, Bosselaers J, Pauwels E, Van Hoorebeke L, Boone M. 2013. X-ray micro-CT
440 reconstruction reveals eight antennomeres in a new fossil taxon that constitutes a sister
441 clade to Dundoxenos and Triozocera (Strepsiptera: Corioxenidae). *Palaeontologia*
442 *Electronica* 16(3):16-31.
- 443 Henwood A. 1992a. Exceptional preservation of dipteran flight muscle and the taphonomy of
444 insects in amber. *Palaios* 7(2):203-212.
- 445 Henwood A. 1992b. Soft-part preservation of beetles in Tertiary amber from the Dominican
446 Republic. *Palaeontology* 35(4):901-912.
- 447 Kirejtshuk AG, Azar D, Tafforeau P, Boistel R, Fernandez V. 2009. New beetles of Polyphaga
448 (Coleoptera, Polyphaga) from Lower Cretaceous Lebanese amber. *Denisia* 26:119-130.
- 449 Krynicki VE. 2013. Primitive ants (Hymenoptera: Sphecomyrminae) in the Campanian (Late
450 Cretaceous) of North Carolina (USA). *Life: The Excitement of Biology* 1:156-165.
- 451 Lak M, Néraudeau D, Nel A, Cloetens P, Perrichot V, Tafforeau P. 2008. Phase contrast X-ray
452 synchrotron imaging: opening access to fossil inclusions in opaque amber. *Microscopy*
453 *and Microanalysis*. 14:251-259.
- 454 McNamara M, Orr PJ, Kearns SL, Alcalá L, Anadón P, Peñalver-Mollá E. 2010. Organic
455 preservation of fossil musculature with ultracellular detail. *Proceedings of the Royal*
456 *Society of London B: Biological Sciences* 277:423–427.
- 457 Solé VA, Papillon E, Cotte M, Walter Ph, Susini J. 2007. A multiplatform code for the analysis of
458 energy-dispersive X-ray fluorescence spectra. *Spectrochim. Acta Part B* 62: 63-68.
- 459 Soriano C, Archer M, Azar D, Creaser P, Delclòs X, Godthelp H, Hand S, Jones A, Nel A,
460 Néraudeau D, Ortega-Blanco J. 2010. Synchrotron X-ray imaging of inclusions in amber.
461 *Comptes Rendus Palevol* 9(6):361-368.
- 462 Speranza M, Wierzchos J, Alonso J, Bettuchi L, Martín-González A, Ascaso C. 2010. Traditional
463 and new microscopy techniques applied to the study of microscopic fungi included in
464 amber. *Microscopy: Science, Technology, Application and Education* 2:1135-1145.
- 465 Tafforeau P, Boistel R, Boller E, Bravin A, Brunet M, Chaimanee Y, Cloetens P, Feist M,
466 Hoszowska J, Jaeger JJ, Kay RF. 2006. Applications of X-ray synchrotron
467 microtomography for non-destructive 3D studies of paleontological specimens. *Applied*
468 *Physics A* 83(2):195-202.
- 469 Tolhurst T, Barbi M, Tokaryk T. 2015. Effective beam method for element concentrations. *J.*
470 *Synchrotron Rad.* 22: 393-399.

- 471 Van de Kamp T, Rolo S, Baumbach T. 2014. Scanning the past—synchrotron X-ray
472 microtomography of fossil wasps in amber. *Entomologie heute* 26:151-160.
- 473 Weitschat W, Wichard W. 2010. Baltic amber. In: Penney D, ed. *Biodiversity of fossils in amber*
474 *from the major world deposits*. Manchester: Siri Scientific Press, 80-115.
- 475 Wogelius RA, Manning PL, Barden HE, Edwards NP, Webb SM, Sellers WI, Taylor KG, Larson
476 PL, Dodson P, You H, Da-Qing L. 2011. Trace metals as biomarkers for eumelanin
477 pigment in the fossil record. *Science* 333(6049):1622-1626.